

Relations between Some Horizontal-Component Ground-Motion Intensity Measures Used in Practice

by David M. Boore and Tadahiro Kishida

Abstract Various measures using the two horizontal components of recorded ground motions have been used in a number of studies that derive ground-motion prediction equations and construct maps of shaking intensity. We update relations between a number of these measures, including those in [Boore *et al.* \(2006\)](#) and [Boore \(2010\)](#), using the large and carefully constructed global database of ground motions from crustal earthquakes in active tectonic regions developed as part of the Pacific Earthquake Engineering Research Center–Next Generation Attenuation–West2 project. The ratios from the expanded datasets generally agree to within a few percent of the previously published ratios. We also provide some ratios that were not considered before, some of which will be useful in applications such as constructing Shake-Maps. Finally, we compare two important ratios with those from a large central and eastern North American database and from many records from subduction earthquakes in Japan and Taiwan. In general, the ratios from these regions are within several percent of those from crustal earthquakes in active tectonic regions.

Electronic Supplement: Figures of ground-motion intensity measure (GMIM) ratios, and csv files with average ratios and the coefficients of fits to the ratios.

Introduction

The two horizontal components of recorded ground motions have been combined in a number of ways to produce ground-motion intensity measures (IMs) used in practice. For example, several early ground-motion prediction equations (GMPEs) used the geometric mean of the motions on the two components (e.g., [Boore *et al.*, 1997](#)). The Pacific Earthquake Engineering Research Center’s (PEER) Next Generation Attenuation (NGA)–West1 project used GMRotI50, introduced by [Boore *et al.* \(2006\)](#), whereas the PEER NGA–West2 project used RotD50 ([Boore, 2010](#)). The maps of shaking intensity developed by the ShakeMap project ([Wald *et al.*, 1999](#)) use the larger of the two components ([Worden and Wald, 2016](#)). Table 1 gives the definitions of the various IMs considered in this article. It is often necessary to convert from one IM to another, and for this reason conversions between a number of these IMs have been published, either graphically or as equations (e.g., [Beyer and Bommer, 2006](#); [Watson-Lamprey and Boore, 2007](#); [Boore, 2010](#); [Shahi and Baker, 2013, 2014](#); [Bradley and Baker, 2015](#)). In this article, we revisit many of these conversions, using the extensive and carefully developed database of the PEER NGA–West2 project, for which the records are from shallow crustal earthquakes in active tectonic regions. We also compare the results with those from the databases being developed for the ongoing PEER NGA–East and NGA–Subduction projects. We concen-

trate on the NGA–West2 database for several reasons: (1) the database spans a wide range of distances and magnitudes, and (2) more GMPEs have been published for shallow crustal earthquakes in tectonically active regions than for stable continental regions (the focus of the NGA–East project) or for subduction regions, and thus there is a greater need to provide conversions between various horizontal-component IMs developed for shallow crustal earthquakes in tectonically active regions.

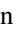
Results: NGA–West2

We computed the various IMs of 21,496 pairs of horizontal-component time series collected for the NGA–West2 database ([Ancheta *et al.*, 2014](#)) for earthquakes ranging in magnitude from 2.99 to 7.9, recorded at distances up to 1533 km. For GMRotI50, the upper limit of the penalty function (see [Boore *et al.*, 2006](#), their equation 4) was taken to be the maximum usable period for each record. This differs from previous work, such as the NGA–West1 project, which used a fixed value of 10 s. Unpublished notes by the first author (see [Data and Resources](#)) find that GMRotI50 is largely insensitive to whether a fixed value of the upper limit is used or whether an upper limit given by the maximum usable period (the inverse of the lowest usable frequency) is used. For each period, we computed the ratios of the different

Table 1
Definitions of Intensity Measures (IMs)

Symbol	Definition*	Beyer and Bommer (2006) Symbol	Bradley and Baker (2015) Symbol
GM _{AR}	Geometric mean of as-recorded horizontal components	GM _{xy}	SA _{GM}
GMRotI50	Median value of the geometric mean of the two horizontal components rotated through all nonredundant period-independent angles (Boore <i>et al.</i> , 2006)	GMRotI50	No equivalences
RotDxx	xx percentile values of response spectra of the two horizontal components projected onto all nonredundant azimuths (Boore, 2010). xx = 00, 50, and 100 correspond to the smallest median, and the largest possible values, respectively	MaxD (equivalent to RotD100; equivalences for RotD00 and RotD50 are not used by Beyer and Bommer)	SA _{RotDxx} (xx = 50 and 100; xx = 00 not used)
Larger	The larger of the two as recorded horizontal components (max (H1,H2))	Env	SA _{Larger}

*The definitions apply to peak ground acceleration (PGA), peak ground velocity (PGV), and pseudoabsolute response spectral acceleration (PSA).

IMs from each pair of records, and then for various subsets of the data defined by ranges of magnitude and distance we computed the geometric mean value of the ratios. We made no distinction between records from mainshocks and aftershocks. We did not use a mixed-effects analysis, because it is likely that any process that produced an event-specific change in the IMs would be canceled out when the ratios were computed; the results of Shahi and Baker (2014) bear this out—they found that the interevent standard deviations from a mixed-effects analysis are very small compared with the intraevent standard deviations. The tables of ratios have been put into the  electronic supplement to this article. These tables include results for peak velocity and peak acceleration, in addition to pseudoabsolute response spectral acceleration (PSA). The figures and tables in this article only show results for PSA.

The magnitude–distance distribution of the NGA-West2 data used in this article is shown in Figure 1, along with that of the NGA-West1 data used by Boore (2010). The NGA-West2 data significantly increase the available data for small earthquakes and for longer periods. Figure 2 shows two ratios that we think are particularly important: RotD50/GMRotI50 and RotD100/RotD50. RotD50/GMRotI50 is useful because it allows for a comparison between the NGA-West1 GMPEs, which used GMRotI50 as the IM, with those of NGA-West2, which used RotD50. The ratio RotD100/RotD50 is used in engineering practice, as discussed, for example, by Shahi and Baker (2014). The ratios are plotted against period in Figure 2, with different symbols used for ratios corresponding to each of five one-magnitude-unit bins. The bars are 95% confidence intervals of the mean ratios. The solid gray line in each graph shows ratios computed for all magnitudes. Only data at distances less than or equal to 200 km were used, because this is the effective upper-distance limit for data from NGA-West1 (see Fig. 1), and one purpose of this article is to compare the results from the NGA-West1 database (as found in the work reported by Boore, 2010) with the much more extensive NGA-West2 database. The NGA-West1 results are shown by the solid dark line in Figure 2. Most of the NGA-West2 GMPEs

are applicable up to distances of 300 km, but often data to 400 km were used in the development of the GMPEs. We repeated most of the analysis using an upper limit of 100 km and found results similar to those when the upper limit was 400 km, as shown in Figure 3 for RotD50/GMRotI50 and three magnitude bins, although there is a small but noticeable dependence of the ratios on distance, as discussed later.

For the NGA-West2 data, the ratios for all magnitudes are similar to those from the smaller events at short periods and are similar to those from the larger events at longer periods. This is because there are many more small-magnitude data at short periods and vice versa at long periods (because the low-cut filters used in processing the records limit the long-period data available for small events). The relative number of available data is shown in Figure 4, for earthquakes less than and greater than M 5.5.

Both ratios shown in Figure 2 (RotD50/GMRotI50 and RotD100/RotD50) are similar for both the NGA-West 2 database and the much smaller NGA-West1 database, particularly for the magnitude 6–7 bin, which is well represented in the NGA-West1 database. The ratios RotD100/RotD50 computed for events of all magnitudes are in good agreement with the trends given by Shahi and Baker (2014, short-dashed lines in Fig. 2), which is not surprising because they also used data from the NGA-West2 project.

As shown in Figures 2 and 3, there is a clear, although small, dependence of the ratios on magnitude and distance (this is also true of other ratios, as subsequent figures will show). Watson-Lamprey and Boore (2007) also found similar dependencies. To capture this effect, we did a regression analysis with various functions, finally settling on this function:

$$\ln(\text{Ratio}) = c_0 + r_1 \ln(R_{\text{RUP}}/50) + m_1(\mathbf{M} - 5.5) + m_2(\mathbf{M} - 5.5)^2, \tag{1}$$

in which the predictor variables are moment magnitude (\mathbf{M}) and the closest distance to the rupture surface (R_{RUP}). The values for these parameters came from the databases and are the results of careful analyses by database working groups for

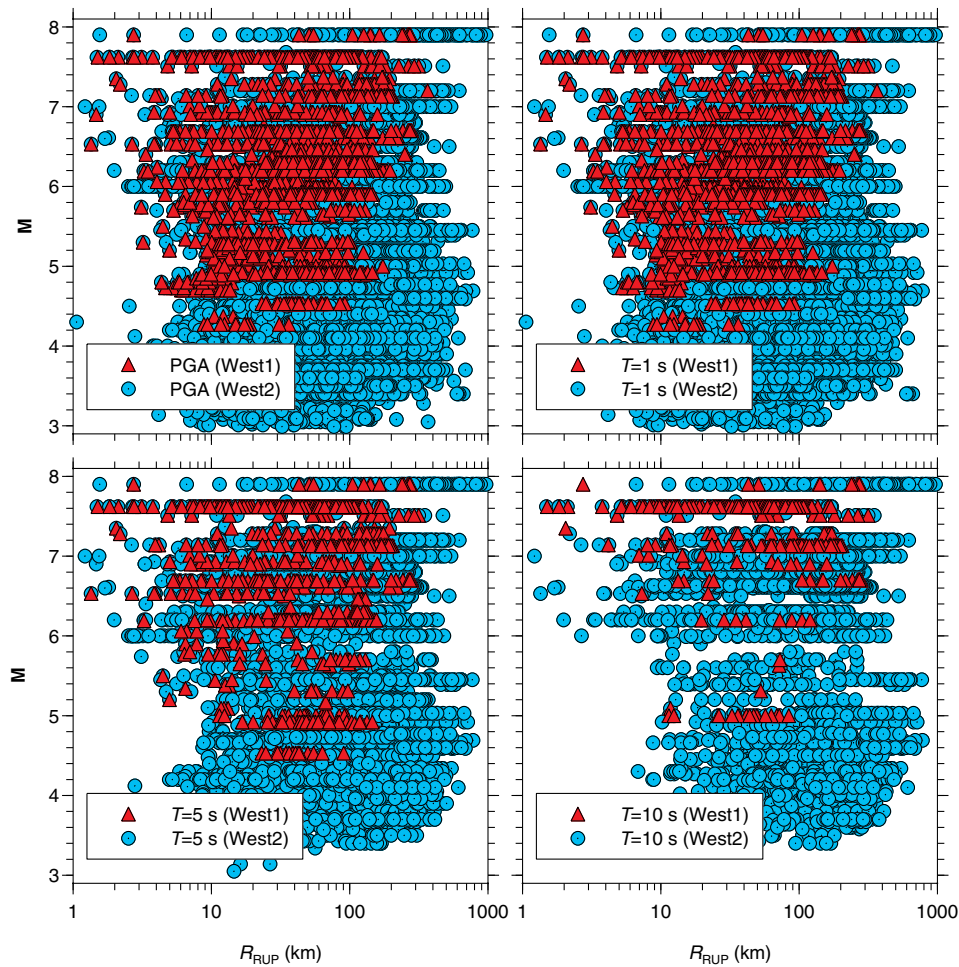


Figure 1. The magnitude–distance distribution of data for the Next Generation Attenuation (NGA)-West1 database used by Boore (2010) and the NGA-West2 database used in this article, for peak ground acceleration (PGA) and pseudoabsolute response spectral acceleration (PSA) at periods of 1, 5, and 10 s. The color version of this figure is available only in the electronic edition.

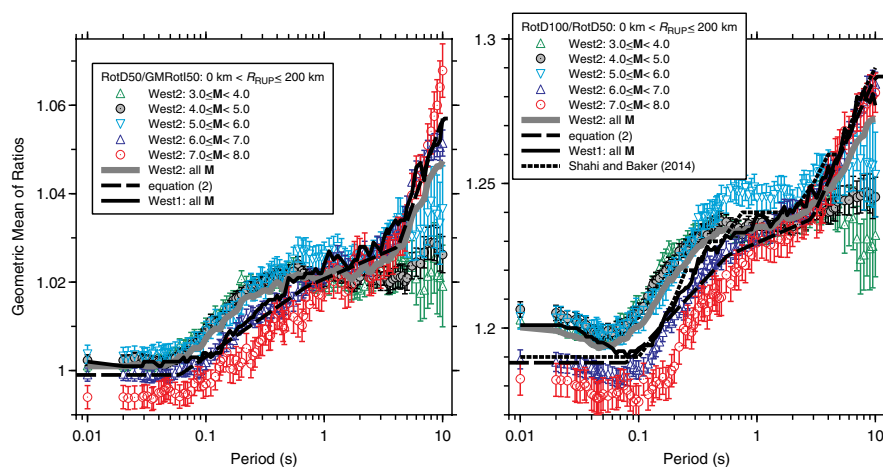


Figure 2. The RotD50/GMRotI50 and RotD100/RotD50 ratios for all events and for five magnitude bins, as well as all magnitude bins combined (all M , the same as $3.0 \leq M < 8.0$). The indicated distance restrictions apply only to the NGA-West2 ratios. The NGA-West2 ratios are the geometric means of the ratios for each record, with the 95% confidence intervals given by the bars. For comparison, the values for all events computed from the NGA-West1 database are also shown (with no restriction on R_{RUP} or M), as are those from Shahi and Baker (2014) and the approximate fit given by equation (2), with coefficients from Table 2, based on the NGA-West2 ratios within 200 km. The color version of this figure is available only in the electronic edition.

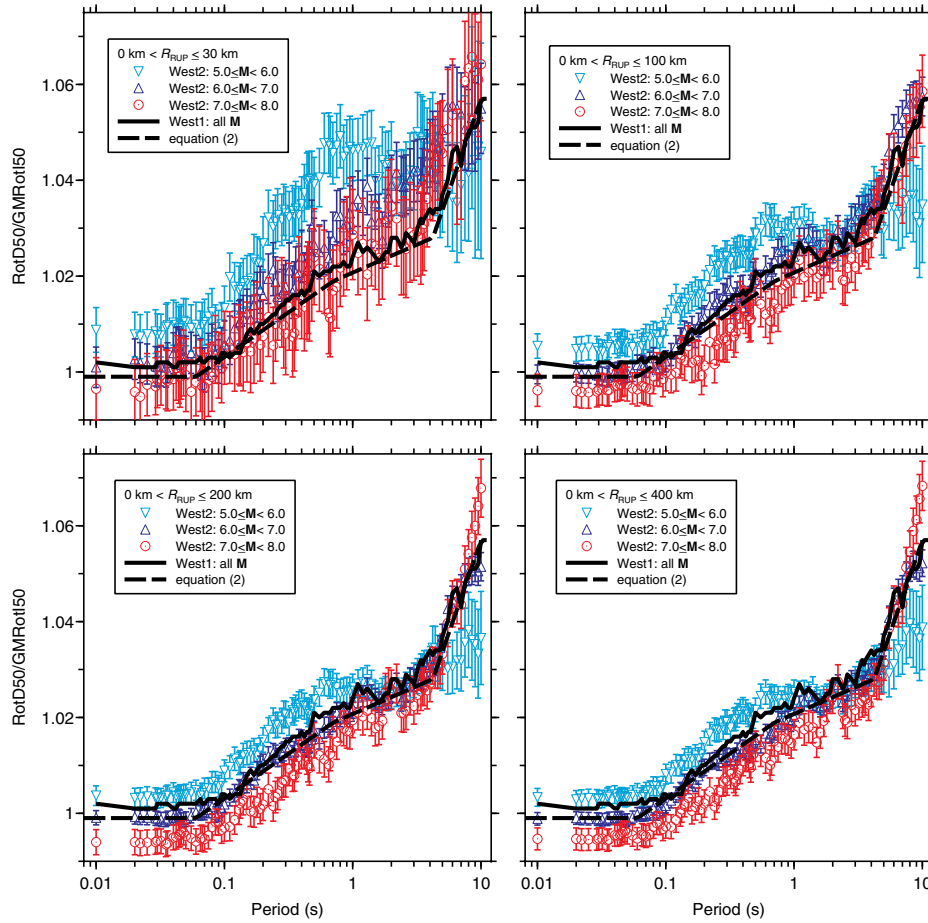


Figure 3. The RotD50/GMRotI50 ratios for three magnitude bins and rupture distances (R_{RUP}) less than or equal to 30, 100, 200, and 400 km. The values shown are the geometric means of the ratios for each record, with the 95% confidence intervals given by the bars. For comparison, the values for all events computed from the NGA-West1 database are also shown (with no restriction on R_{RUP} or M), along with the approximate fit given by equation (2), with coefficients from Table 2, based on the NGA-West2 ratios within 200 km. The color version of this figure is available only in the electronic edition.

each NGA project. If not directly available (e.g., M for small earthquakes), the values were estimated from other available information (e.g., conversions between various magnitudes). The coefficients of equation (1), which were determined for each period independently, are given for nine ratios in the $\text{\textcircled{E}}$ electronic supplement to this article. There is a very large scatter in the ratios, and the dependence on magnitude and distances is small, as shown in Figure 5 for RotD100/RotD50 as a function of R_{RUP} for M near 6.5 and as a function of M for R_{RUP} near 50 km. As a result of the large scatter and small dependence on R_{RUP} and M , the reduction in variance due to the regression is almost negligible. The regression coefficients, however, are statistically significant. As an alternative to using this equation for determining the cases of practical importance for the ratio, we computed the ratios for events with $M \geq 5.0$ and found that a series of straight lines provided a good fit to the ratios. There is precedent for using period-dependent but magnitude- and distance-independent straight line segments to represent the ratios (e.g., [Beyer and Bommer, 2006](#); [Shahi and Baker, 2014](#); [Bradley and Baker, 2015](#)).

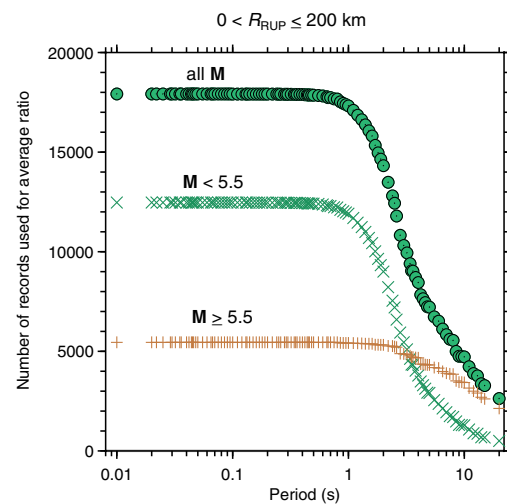


Figure 4. The number of records for the NGA-West2 database, plotted as a function of period, used in computing the ratios. The numbers of records are shown for all events and for those with magnitudes less than and greater than 5.5. The color version of this figure is available only in the electronic edition.

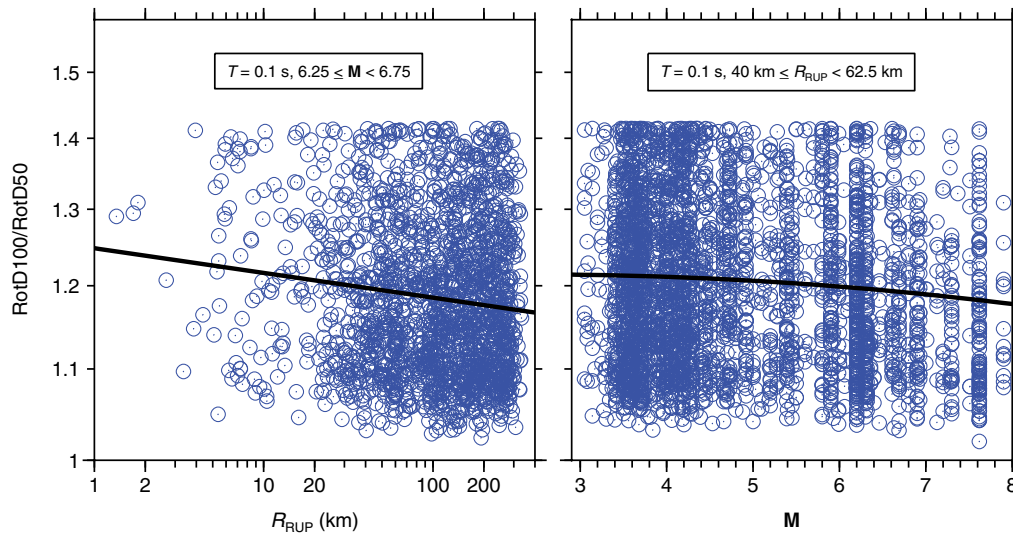


Figure 5. The individual RotD100/RotD50 ratios (not the means) for PSA at 0.1 s as a function of R_{RUP} for M within 0.25 units of 6.5, and as a function of M for R_{RUP} within a factor of 1.25 of 50 km. The predictions from the regression fit of equation (1) to the whole dataset are also shown. The color version of this figure is available only in the electronic edition.

These lines are given in the following compact form, with coefficients given in Table 2:

$$\begin{aligned} \text{Ratio} = \max & \left(R_1, \max \left\{ \min \left[R_1 + \frac{(R_2 - R_1)}{\ln(T_2/T_1)} \ln(T/T_1), \right. \right. \right. \\ & \times R_2 + \left. \left. \frac{(R_3 - R_2)}{\ln(T_3/T_2)} \ln(T/T_2) \right] \right\}, \right. \\ & \left. \times \min \left[R_3 + \frac{(R_4 - R_3)}{\ln(T_4/T_3)} \ln(T/T_3), R_5 \right] \right) \Bigg), T \leq 10 \text{ s.} \end{aligned} \quad (2)$$

The coefficients were determined subjectively, guided largely by the magnitude 6–7 ratios. The resulting line-segment representation is included in Figure 2 for RotD50/GMRot50 and RotD100/RotD50; subsequent figures include the line-segment approximation for other ratios. We note that the error in ignoring the magnitude dependence is only about 1%–3%, although it looks worse than this because of the expanded ordinate scale in Figure 2 (and subsequent figures).

The tables of average ratios used as the basis for the above equations are given in the $\text{\textcircled{E}}$ electronic supplement. Those tables also contain the standard deviations of the ratios for possible use in determining the standard deviations of

motions obtained using the ratios to convert from one IM to another, as discussed in detail by Beyer and Bommer (2006). The distributions of the logarithms of the ratios, however, are seldom well approximated by a normal distribution (see also Beyer and Bommer, 2006) and thus should be used with caution.

One thing not included in the tables is the correlation coefficient between the ratio of IMs and the IM in the denominator of the ratio. This coefficient is used in the formal determination of the uncertainty in IM Y_2 , given Y_1 and the ratio Y_2/Y_1 , according to the following equation from Watson-Lamprey and Boore (2007):

$$\sigma_{\ln Y_2}^2 = \sigma_{\ln Y_1}^2 + \sigma_{\ln(Y_2/Y_1)}^2 + 2r_{Y_1, Y_2/Y_1} \sigma_{\ln Y_1} \sigma_{\ln(Y_2/Y_1)}, \quad (3)$$

in which σ denotes the standard deviations of the indicated quantities, and $r_{Y_1, Y_2/Y_1}$ is the correlation coefficient between $\ln Y_1$ and $\ln(Y_2/Y_1)$. In this equation, Y_1 , Y_2 , and Y_2/Y_1 have all been adjusted for dependence on predictor variables, such as magnitude and distance. We have not included the correlation coefficient for two reasons: (1) it requires a GMPE for Y_1 , and this is not always available for the various Y_1 IMs; and (2) more importantly, in one case we studied (Y_1 and Y_2 being RotD50 and RotD100, respectively), the

Table 2
Coefficients of Equation (2) Line Approximations to Ratios for $R_{RUP} \leq 200$ km

Ratio	RotD50/GMRot50		RotD50/GM _{AR}		RotD100/RotD50		Larger/GMRot50		Larger/GM _{AR}		Larger/RotD50	
	T_i	R_i	T_i	R_i	T_i	R_i	T_i	R_i	T_i	R_i	T_i	R_i
1	0.06	0.999	0.09	1.009	0.12	1.188	0.08	1.106	0.10	1.117	0.10	1.107
2	0.71	1.019	0.58	1.028	0.41	1.225	0.56	1.158	0.53	1.165	0.45	1.133
3	4.21	1.028	4.59	1.042	3.14	1.241	4.40	1.178	4.48	1.195	4.36	1.149
4	10.00	1.057	8.93	1.077	10.00	1.287	8.70	1.241	8.70	1.266	8.78	1.178
5	—	1.057	—	1.077	—	1.287	—	1.241	—	1.266	—	1.178

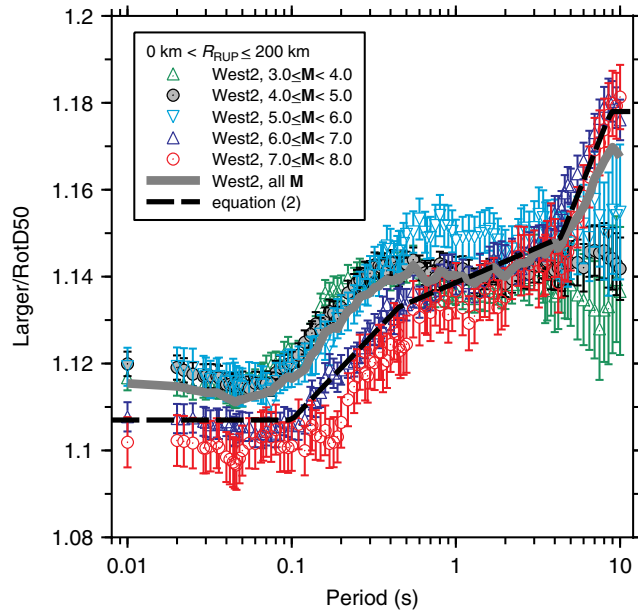


Figure 6. The Larger/RotD50 ratios for all events and for five magnitude bins, as well as all magnitudes bins combined (all M , the same as $3.0 \leq M < 8.0$). The rupture distances (R_{RUP}) were less than or equal to 200 km. The values shown are the geometric means of the ratios for each record, with the 95% confidence intervals given by the bars. The approximate fit given by equation (2), with coefficients from Table 2, is also shown. The color version of this figure is available only in the electronic edition.

correlation coefficient is small, and the contribution to $\sigma_{\ln Y2}$ is dominated by $\sigma_{\ln Y1}$. This is shown in Table 3, in which including the standard deviation of the ratio only increases the standard deviation of $\ln Y2$ by about 1% over the standard deviation of $\ln Y1$, and the standard deviations of $\ln Y2$ computed with and without the correlation coefficient are very similar.

Ratios involving the Larger IM are of interest because some older GMPEs may have used this IM. More importantly,

the data that form the basis for ShakeMaps (Wald *et al.*, 1999) use this IM, but GMPEs developed for other IMs are used in addition to the data when making the maps, and therefore a conversion from the GMPE IM to the Larger IM needs to be made (Worden and Wald, 2016; E. Thompson, personal comm., 2016). Figure 6 shows the Larger/RotD50 ratio, and the $\text{\textcircled{E}}$ electronic supplement contains ratios of Larger to GMRot50, GM_{AR} , RotD50, and RotD100. A figure of Larger/RotD100 is also included in the $\text{\textcircled{E}}$ electronic supplement; this figure shows that Larger/RotD100 is always less than unity, as it must be, given the definition of RotD100.

Figure 7, our final set of graphs using only the NGA-West2 data, shows ratios involving the GM_{AR} IM: RotD50/ GM_{AR} and Larger/ GM_{AR} . We show the ratios computed for two ranges of distance, with $R_{RUP} \leq 200$ km, as in the previous figures, and $R_{RUP} \leq 30$ km. The latter distance was used because we wanted to compare our results with those from Bradley and Baker (2015), who used data from 10 Christchurch, New Zealand, earthquakes with magnitudes between 4.7 and 7.1, recorded at distances within 50 km (with one exception, for which 100 km was the maximum distance; Bradley, 2015). The results of Bradley and Baker (2015) are generally within 2%–3% of our results for almost all periods, even though the expanded ordinate scale makes it appear that the agreement is worse than this. The comparison of the ratios from the NGA-West2 data with those from the NGA-West1 data (a dataset also used by Beyer and Bommer, 2006) is better for the larger range of distances. This is as it should be, given that the NGA-West1 results are based on data to about 200 km.

Comparison of NGA-West2 Ratios with Those from Other Regions

As part of ongoing PEER NGA projects for central and eastern North America (NGA-East) and subduction regions (NGA-Subduction), large databases are being developed (see Data and Resources). The magnitude and distance distribution

Table 3
Quantities Associated with the Determination of Uncertainties in Intensity Measure $Y2$, Given $Y1$, and the Ratio $Y2/Y1$

Per(s)	Nrecs	SigY2/Y1	SigY1	CorY2/Y1, Y1	SigY2total	SigY2xcor	SigY2total/SigY1	SigY2 : total/xcor
0	21083	0.0837	0.877	0.077	0.888	0.881	1.012	1.007
0.1	21079	0.0813	0.992	0.097	1.003	0.995	1.011	1.008
0.2	21064	0.0829	0.923	0.122	0.937	0.927	1.015	1.011
0.4	21039	0.0837	0.856	0.095	0.868	0.860	1.014	1.009
0.8	20809	0.0836	0.835	0.052	0.843	0.839	1.010	1.005
1.6	18848	0.0843	0.839	0.042	0.847	0.844	1.009	1.004
3.2	12260	0.0844	0.802	0.067	0.812	0.806	1.013	1.007
6.5	7909	0.0827	0.784	0.179	0.803	0.789	1.024	1.018

Per(s), Period in seconds; Nrecs, number of records used in the residual analysis; SigY2/Y1, standard deviation of $\ln(Y2/Y1)$, after adjustment for M and R_{RUP} dependence; SigY1, the standard deviation of $\ln Y1$, after adjustment for M , R_{JB} , and V_{S30} dependence using the equations of Boore *et al.* (2014); CorY2/Y1, Y1, the correlation coefficient of $\ln Y2/Y1$ and $\ln Y1$, after adjustment for the relevant predictor variables; SigY2total, the standard deviation of $\ln Y2$, from equation (3); SigY2xcor, the standard deviation of $\ln Y2$, from equation (3) without the term involving the correlation coefficient; SigY2total/SigY1, the ratio of the standard deviations of $\ln Y2$, using equation (3), and $\ln Y1$; SigY2, total/xcor, the ratio of the standard deviations with and without the correlation coefficient term.

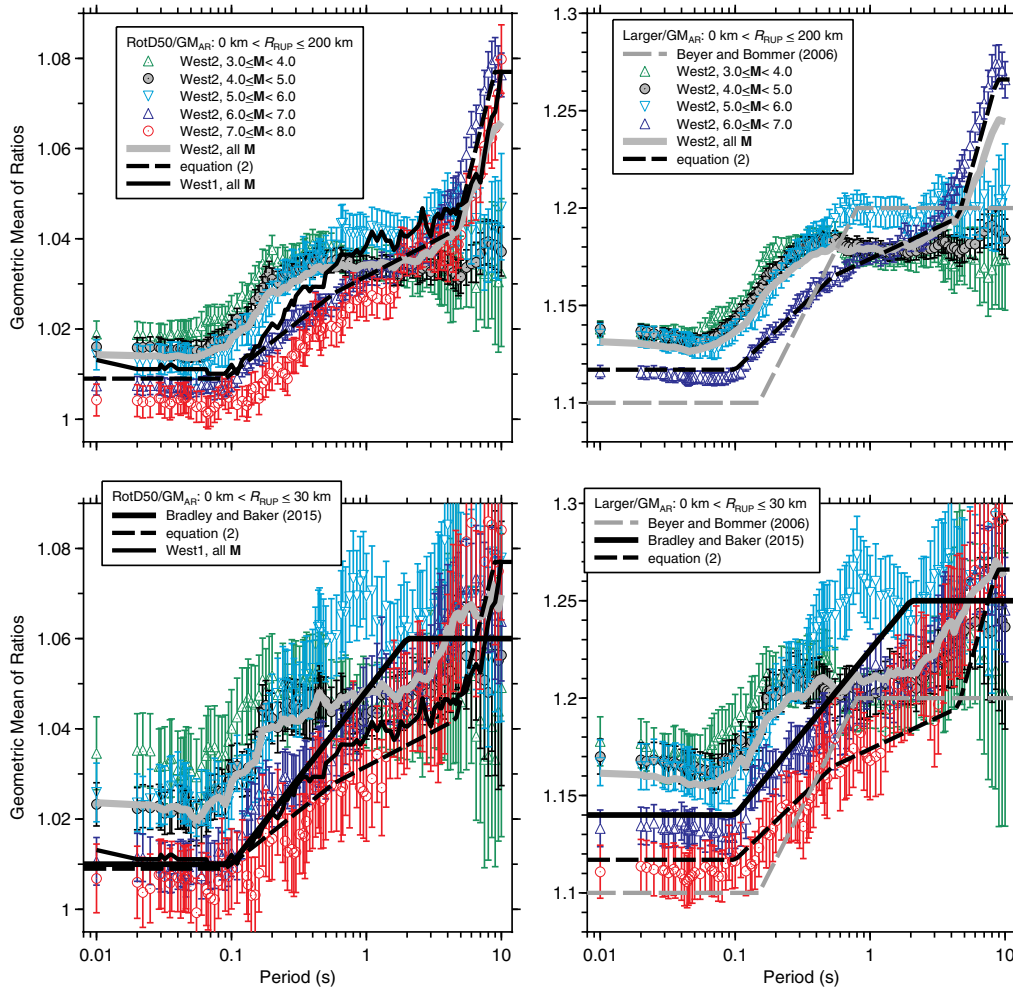


Figure 7. The RotD50/GM_{AR} and Larger/GM_{AR} ratios for all events and for five magnitude bins, as well as all magnitude bins combined (all M, the same as $3.0 \leq M < 8.0$). The rupture distances (R_{RUP}) were less than or equal to 200 km (top row) and 30 km (bottom row). The ratios from the NGA-West2 database are the geometric means of the ratios for each record, with the 95% confidence intervals given by the bars. The approximate fit given by equation (2), with coefficients from Table 2, is also shown, as are relations published by Beyer and Bommer (2006) for Larger/GM_{AR} and Bradley and Baker (2015) for RotD50/GM_{AR} and Larger/GM_{AR} for R_{RUP} less than 30 km. For comparison, the figure also shows RotD50/GM_{AR} computed from the NGA-West1 database for all M and R_{RUP} . The color version of this figure is available only in the electronic edition.

for these databases are compared with the NGA-West2 database in Figure 8 (we show data for two subduction regions: Japan and Taiwan). The NGA-East and the subduction databases overlap different subregions of the NGA-West2 database (we are ignoring depths here), but in general each of the three new datasets have a significant number of recordings in the R_{RUP} range of 100–400 km. We compare the average RotD50/GM_{Rot150} and RotD100/RotD50 ratios for this distance range in Figures 9 and 10, respectively. For the Taiwan subduction data, we only used the broadband Taiwan (TW) network data for the magnitude 4–5 range, because the Central Weather Bureau (CWB) accelerometer array is limited in the smallest recorded accelerations; we used both the TW and CWB network data for the two larger magnitude bins. With the exception of longer periods and the magnitude 5–6 data from the NGA-East database, the ratios from the four databases are quite similar to one another, even though the nature of the

earthquakes and the site conditions can be quite different (we make no attempt in this study to look at site-condition dependence of the ratios). We have no explanation for the inconsistency for the magnitude 5–6 ratios for NGA-East, although the ratios come from a relatively small number of recordings and earthquakes (148 records from five earthquakes for $T = 0.1$ s, and 98 records from four earthquakes for $T = 10$ s). For this reason, the mean ratios are not as well determined as for the ratios from the other magnitude ranges (which have more data), but the 95% confidence intervals shown on the graphs formally suggest that the discrepancy is significant. We point out, however, that the discrepancy is only about 3%.

Discussion

We present various IM ratios obtained from the extensive NGA-West2 database. Some of these ratios have not

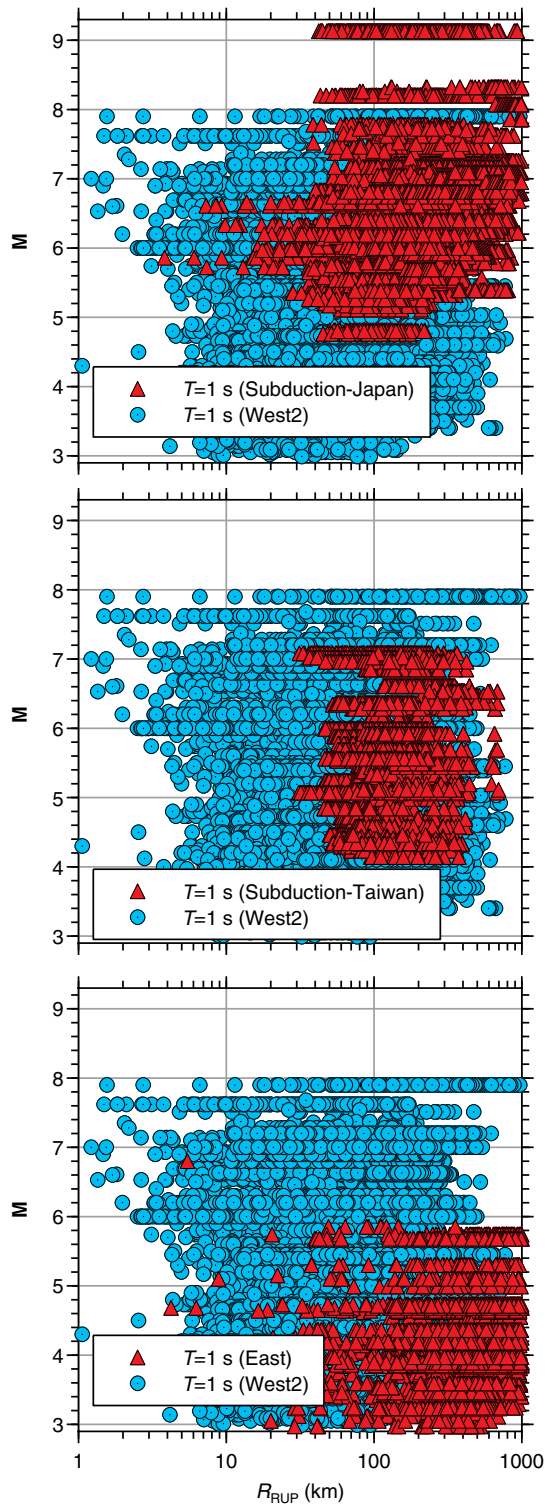


Figure 8. The magnitude–distance distribution of 1 s PSA for the NGA-West2 database, compared with that for data from eastern North America (East) and subduction earthquakes in Japan and Taiwan. The color version of this figure is available only in the electronic edition.

been provided in previous publications, but for the others, our results are similar to those given before. We also find that the ratios are generally similar to those from earthquakes

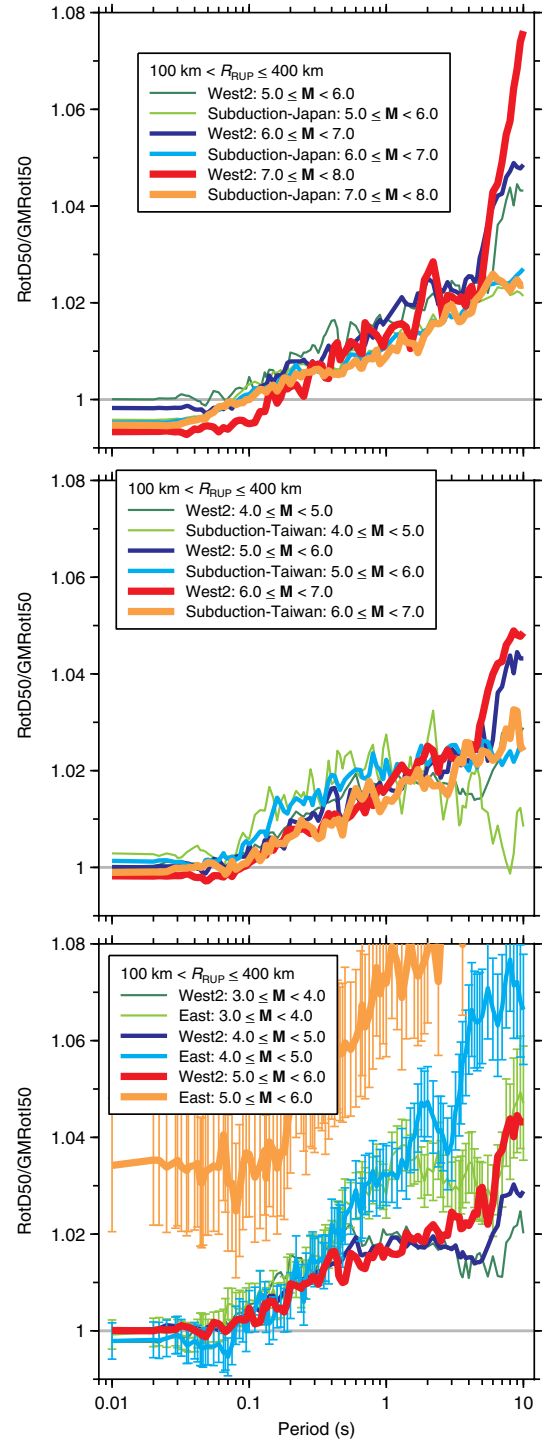


Figure 9. The $RotD50/GMRotI50$ ratios, for the indicated magnitude bins, for four datasets (West2, Subduction-Japan, Subduction-Taiwan, and East). The rupture distances (R_{RUP}) were between 100 and 400 km. The ratios are the geometric means of the ratios for each record. 95% confidence limits are shown for the East ratios; we added these to see if the differences between the M 5–6 ratios and the ratios for the other magnitude bins for East, as well as the differences between the East and West2 ratios at longer periods, were statistically significant. The color version of this figure is available only in the electronic edition.

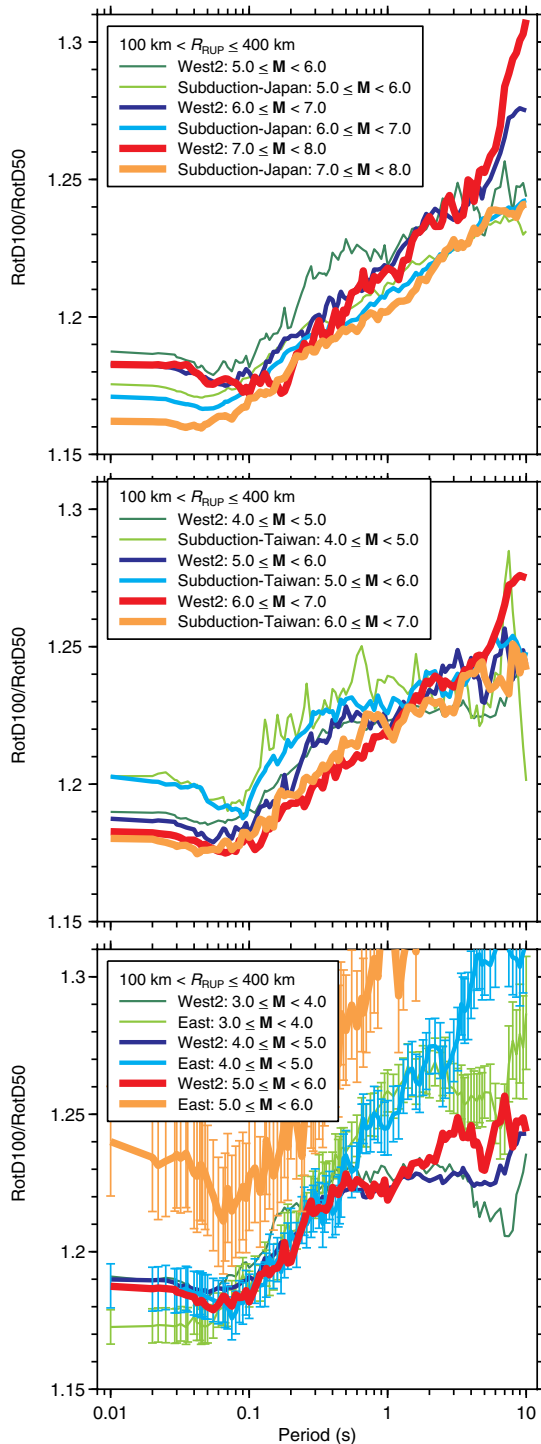


Figure 10. The RotD100/RotD50 ratios for the indicated magnitude bins, for four datasets (West2, Subduction-Japan, Subduction-Taiwan, and East). The rupture distances (R_{RUP}) were between 100 and 400 km. The ratios are the geometric means of the ratios for each record. 95% confidence limits are shown for the East ratios; we added these to see if the differences between the M 5–6 ratios and the ratios for the other magnitude bins for East, as well as the differences between the East and West2 ratios at longer periods, were statistically significant. The color version of this figure is available only in the electronic edition.

in central and eastern North America, a stable continental region, and subduction earthquakes in Japan and Taiwan. There is a small magnitude and distance dependence to the ratios, and we provide coefficients for an equation relating the ratios to magnitude and distance. We also provide coefficients for a period-dependent multi-line-segment representation of the ratios that are independent of magnitude and distance. The error in converting between IMs using this representation, and thus ignoring the magnitude and distance dependence, is generally less than 2%.

Data and Resources

The Next Generation Attenuation (NGA)-West2 intensity measures (IMs) were computed from time series collected as part of the Pacific Earthquake Engineering Research Center (PEER) NGA-West2 project (<http://peer.berkeley.edu/ngawest2/databases>, last accessed September 2016). The IMs used to compute ratios for East, Subduction-Japan, and Subduction-Taiwan were computed from time series collected as part of the ongoing NGA-East and NGA-Subduction projects. We used data available as of late June 2016. The IMs were computed using an adaptation of the program *smc2psa_rot_gmrot_interp_acc_rot_osc_ts*, part of the TSPP (Time-Series Processing Programs) suite of programs available from the online software link on <http://www.daveboore.com> (last accessed September 2016); their use is described in Boore (2015). A study of the sensitivity of GMRotI50 to the choice of the upper-period limit used in computing the penalty function is given in *some_notes_on_Tmax_for_GMRotI50_penalty_function.pdf*, available from http://www.daveboore.com/daves_notes.html (last accessed September 2016). The bulk of the data analysis was done using the program R, available from <http://www.r-project.org/> (last accessed September 2016), and many of the figures were prepared using CoPlot (www.cohort.com, last accessed September 2016).

Acknowledgments

We thank Emel Seyhan for prompting this research by asking the first author if results presented at a workshop in 2012 superseded those in Boore (2010). Eric Thompson pointed out that ratios involving the Larger IM were useful in ShakeMap. We thank Brendon Bradley, Suzanne Hecker, Emel Seyhan, and Eric Thompson for careful reviews of the article.

References

- Ancheta, T. D., R. B. Darragh, J. P. Stewart, E. Seyhan, W. J. Silva, B. S. J. Chiou, K. E. Wooddell, R. W. Graves, A. R. Kottke, D. M. Boore, *et al.* (2014). NGA-West2 database, *Earthq. Spectra* **30**, 989–1005.
- Beyer, K., and J. J. Bommer (2006). Relationships between median values and between aleatory variabilities for different definitions of the horizontal component of motion, *Bull. Seismol. Soc. Am.* **96**, 1512–1522.
- Boore, D. M. (2010). Orientation-independent, non geometric-mean measures of seismic intensity from two horizontal components of motion, *Bull. Seismol. Soc. Am.* **100**, 1830–1835.
- Boore, D. M. (2015). TSPP—A collection of FORTRAN programs for processing and manipulating time series, *U.S. Geol. Surv. Open-File Rept. 2008-1111* (Revision 4.6.2, 4 December 2015), 51 pp.

- Boore, D. M., W. B. Joyner, and T. E. Fumal (1997). Equations for estimating horizontal response spectra and peak acceleration from western North American earthquakes: A summary of recent work, *Seismol. Res. Lett.* **68**, 128–153.
- Boore, D. M., J. P. Stewart, E. Seyhan, and G. M. Atkinson (2014). NGA-West2 equations for predicting PGA, PGV, and 5%-damped PSA for shallow crustal earthquakes, *Earthq. Spectra* **30**, 1057–1085.
- Boore, D. M., J. Watson-Lamprey, and N. A. Abrahamson (2006). Orientation-independent measures of ground motion, *Bull. Seismol. Soc. Am.* **96**, 1502–1511.
- Bradley, B. A. (2015). Systematic ground motion observations in the Canterbury earthquakes and region-specific non-ergodic empirical ground motion modeling, *Earthq. Spectra* **31**, 1735–1761.
- Bradley, B. A., and J. W. Baker (2015). Ground motion directionality in the 2010–2011 Canterbury earthquakes, *Earthq. Eng. Struct. Dynam.* **44**, 371–384.
- Shahi, S. K., and J. W. Baker (2013). NGA-West2 models for ground-motion directionality, *PEER 2013/10*, Pacific Earthquake Engineering Research Center, Berkeley, California, 73 pp.
- Shahi, S. K., and J. W. Baker (2014). NGA-West2 models for ground-motion directionality, *Earthq. Spectra* **30**, 1285–1300.
- Wald, D. J., V. Quitoriano, T. H. Heaton, H. Kanamori, C. W. Scrivner, and C. B. Worden (1999). TriNet “ShakeMaps”: Rapid generation of peak ground motion and intensity maps for earthquakes in southern California, *Earthq. Spectra* **15**, 537–555.
- Watson-Lamprey, J. A., and D. M. Boore (2007). Beyond Sa_{GMROff} : Conversion to Sa_{Arb} , Sa_{SN} , and Sa_{MaxRot} , *Bull. Seismol. Soc. Am.* **97**, 1511–1524.
- Worden, C. B., and D. J. Wald (2016). *ShakeMap Manual*, 1 February 2016, available at <http://usgs.github.io/shakemap> (last accessed February 2016), doi: [10.5066/F7D21VPQ](https://doi.org/10.5066/F7D21VPQ).

U.S. Geological Survey
345 Middlefield Road
Menlo Park, California 94025
boore@usgs.gov
(D.M.B.)

Pacific Earthquake Engineering Research Center
University of California
Berkeley, California 94720
tkishida@berkeley.edu
(T.K.)

Manuscript received 31 July 2016;
Published Online 27 December 2016